

See discussions, stats, and author profiles for this publication at: <https://www.researchgate.net/publication/41893426>

Mechanistic Investigation of the Hydrogenation of O-2 by a Transfer Hydrogenation Catalyst

ARTICLE in JOURNAL OF THE AMERICAN CHEMICAL SOCIETY · MARCH 2010

Impact Factor: 12.11 · DOI: 10.1021/ja908453k · Source: PubMed

CITATIONS

13

READS

48

4 AUTHORS, INCLUDING:



Nino Russo

Università della Calabria

512 PUBLICATIONS 7,995 CITATIONS

[SEE PROFILE](#)



Emilia Sicilia

Università della Calabria

152 PUBLICATIONS 1,949 CITATIONS

[SEE PROFILE](#)

Mechanistic Investigation of the Hydrogenation of O₂ by a Transfer Hydrogenation Catalyst

Sugata Chowdhury,[†] Fahmi Himo,[‡] Nino Russo,[†] and Emilia Sicilia^{*,†}

Dipartimento di Chimica, Università della Calabria, I-87030, Arcavacata di Rende, Italy, and Arrhenius Laboratory, Department of Organic Chemistry, Stockholm University, SE-10691 Stockholm, Sweden

Received October 5, 2009; E-mail: siciliae@unical.it

Abstract: The mechanistic details of the hydrogenation of molecular oxygen by the 18e amino-hydride Cp*IrH(TsDPEN) (**1H(H)**) complex to give Cp*Ir(TsDPEN-H) (**1**) and 1 equiv of H₂O were investigated by means of hybrid density functional calculations (B3LYP). To comprehensively describe the overall catalytic cycle of the hydrogenation of dioxygen using H₂ catalyzed by the Ir complex **1**, the potential energy surfaces for the hydrogenation process of both the catalyst **1** and the corresponding unsaturated iridium(III) amine cation ([**1H**]⁺) were explored at the same level of theory. The results of our computations, in agreement with experimental findings, confirm that the addition of H₂ to the 16e diamido complexes **1** is favorable but is slow and is accelerated by the presence of Brønsted acids, such as HOTf, which convert **1** into the corresponding amine cation [**1H**]⁺. By deprotonation of the subsequently hydrogenated [**1H(H₂)**]⁺ complex the amine hydride catalyst **1H(H)** is generated, which is able to reduce molecular oxygen. Calculations corroborate that the O₂ reduction goes through formation of an intermediate iridium hydroperoxo complex that reacts with **1H(H)** to eliminate water, restore **1**, and restart the catalytic cycle. From the outcomes of our computational analysis it results that the slow step of the overall O₂ hydrogenation process is the O₂ insertion into the Ir–H bond, and the highest calculated barrier along this pathway to give the hydroperoxo product shows a good agreement with the experimentally estimated value. As a consequence, unreacted **1H(H)** approaches **1H(OOH)** to give **1H(OH)** and water according to the experimentally observed second-order kinetics with respect to [**1H(H)**]. Calculations were carried out to explore the possibility that H₂O₂ is released from the hydroperoxo intermediate together with catalyst **1**, and the subsequent water elimination reaction occurs by reduction of produced H₂O₂ with **1H(H)** to regenerate catalyst **1**. Preliminary results concerning the O₂ reduction in acidic conditions show that the reaction proceeds by intermediate production of H₂O₂, which reacts with **1H(H)** to eliminate water, restore [**1H**]⁺, and restart the catalytic cycle. The energetics of the process appear to be definitely more favorable with respect the analogous pathways in neutral conditions.

1. Introduction

Metal hydrido-amine complexes (metal = Ru, Rh, and Ir) developed by Noyori et al.¹ attract ever increasing attention as highly active and enantioselective transfer hydrogenation catalysts. The key feature of most transfer hydrogenation catalysts is the presence of a hydridic M–H subunit adjacent to a protic N–H functionality. In neutral and basic conditions the catalyst transfers these two hydrogen atoms to polar unsaturated substrates, avoiding direct coordination of the substrate to the metal. As a consequence of this hydrogen transfer, the catalyst is converted into a 16-electron amido entity through a six-membered-ring transition state.² Then, in the catalyst regeneration step, dihydrogen sources provide H₂ to the amido complex to re-form the 18-electron amino-hydride. Noyori and co-

workers, more recently, have reported that these compounds are efficient catalysts also in acidic conditions.³ The success of Noyori's catalysts triggered extensive studies of isoelectronic Ru and Ir catalysts developed by Mashima and Ikariya.⁴

In spite of the considerable advances in catalysis, much of the reactivity of such amino-amide complexes beyond use as transfer hydrogenation catalysts remains relatively unexplored. Moreover, the dehydrogenative oxidation properties of such amine/amido systems has been investigated less, mainly due to the lack of appropriate hydrogen acceptor. Ikarya and co-workers successfully demonstrated, in the area of oxidative chiral resolution of secondary alcohols, that molecular oxygen readily reacts with amine-hydrido complexes, leading to the amido complexes.⁵

[†] Università della Calabria.

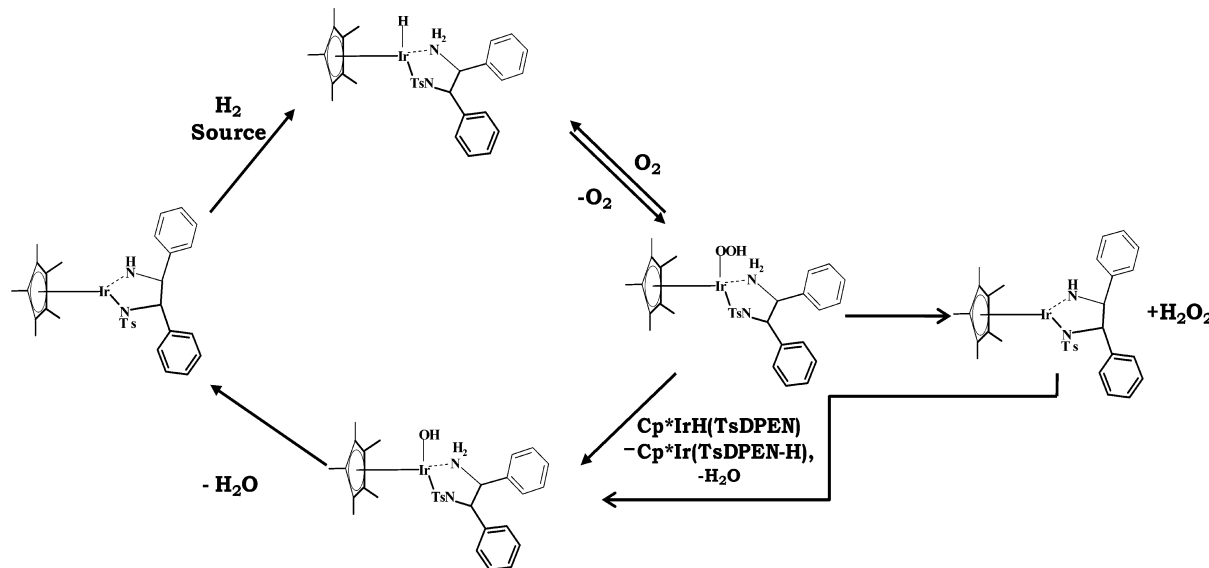
[‡] Stockholm University.

(1) (a) Noyori, R.; Hashiguchi, S. *Acc. Chem. Res.* **1997**, *30*, 97–102. (b) Ikariya, T.; Murata, K.; Noyori, R. *Org. Biomol. Chem.* **2006**, *4*, 393–406.

(2) Yamakawa, M.; Ito, H.; Noyori, R. *J. Am. Chem. Soc.* **2000**, *122*, 1466–1478.

(3) (a) Ohkuma, T.; Utsumi, N.; Tsutsumi, K.; Murata, K.; Sandoval, C.; Noyori, R. *J. Am. Chem. Soc.* **2006**, *128*, 8724–8725. (b) Ohkuma, T.; Tsutsumi, K.; Utsumi, N.; Arai, N.; Noyori, R.; Murata, K. *Org. Lett.* **2007**, *9*, 255–257. (c) Sandoval, C. A.; Ohkuma, T.; Utsumi, N.; Tsutsumi, K.; Murata, K.; Noyori, R. *Chem. Asian J.* **2006**, *1*, 102–110.

(4) (a) Mashima, K.; Abe, T.; Tani, K. *Chem. Lett.* **1998**, 1199–1200. (b) Mashima, K.; Abe, T.; Tani, K. *Chem. Lett.* **1998**, 1201–1202. (c) Murata, K.; Ikariya, T.; Noyori, R. *J. Org. Chem.* **1999**, *64*, 2186.

Scheme 1. Proposed Catalytic Cycle for the Dioxogen Reduction with Cp*IrH(TsDPEN)

In the effort to develop new homogeneous catalysts able to hydrogenate oxygen, Heiden and Rauchfuss⁶ have investigated the possibility to exploit the combined oxidative and reductive properties of such a topical class of transfer hydrogenation catalysts to achieve the catalytic hydrogenation of oxygen to give water. Indeed, only few conventional homogeneous catalysts are reactive toward both molecular hydrogen and oxygen, because complexes that are reactive toward H₂ are quickly and irreversibly oxidized by O₂, whereas complexes that are readily oxidized by O₂ are generally inert toward H₂. In their investigation⁶ the authors have highlighted that metal hydrido-amines can act as homogeneous fuel cells, catalyzing the unusual reduction of dioxygen with hydrogen similar to Knall gas bacteria,⁷ resulting in water as the only byproduct. Specifically, exposure of a solution of the 18e amino-hydride complex Cp*IrH(rac-TsDPEN) (TsDPEN = H₂NCHPhCHPhN-(SO₂C₆H₄CH₃)⁻, Cp* = η⁵-C₅(CH₃)₅) (**1H(H)**) to molecular oxygen resulted in the formation of Cp*Ir(TsDPEN-H) (**1**) and one equivalent of water. Kinetic analysis showed a second-order dependence on [**1H(H)**] and a first-order dependence on [O₂]. Through isotopic labeling experiments, the reaction was found to be localized at the iridium center ($k_{\text{H}}/k_{\text{D}} = 7.1$), indicating that the amine protons ($k_{\text{H}}/k_{\text{D}} = 1.2$) have a secondary effect. The reduction of dioxygen with **1H(H)** was found to be catalytic in the presence of a hydrogen source such as alcohols and ammonia-boranes. The reaction of **1H(H)** with O₂ is proposed to occur by means of formation of a hydroperoxide intermediate, **1H(OOH)**, obtained by direct O₂ insertion into the metal–hydride bond. The same hypothesis was formulated by Ikariya et al.⁵ and is supported by the observation of analogous reactions of molecular oxygen with metal hydrides to produce hydroxides and hydroperoxides.⁸ In particular, Goldberg, Kemp, and co-workers^{8c} reported the first observation of what can be assumed to be an unusual direct insertion of molecular oxygen into a Pd(II)–hydride bond to form a hydroperoxopalladium complex,

for a Pd complex that, due to the nature of the ligand, cannot undergo reductive elimination. Detailed theoretical studies have been carried out to probe the reaction mechanism that involves hydrogen abstraction by O₂ and formation of an OOH fragment that rearranges to give the final hydroperoxo complex.⁹ Subsequently, Stahl and co-workers¹⁰ have reported other examples of Pd complexes undergoing facile conversion to hydroperoxides in the presence of molecular oxygen, and accurate theoretical analyses have been carried out to probe the alternative reaction pathways for the direct and stepwise addition of O₂.¹¹

On the basis of the experimental findings the authors propose that the formed **1H(OOH)** reacts with **1H(H)** to produce **1**, H₂O, and **1H(OH)**. By spontaneous elimination of water from the resulting hydroxy-amine **1H(OH)**, **1** is given, which is poised to be reduced by H₂. Since the rate of dehydrogenation was found to be highly solvent dependent, the experiment was carried out in CH₃CN or CH₂Cl₂ solutions, in which reactions proceeded at rates convenient for mechanistic analysis. In Scheme 1 is sketched the complete catalytic cycle for the hydrogenation of O₂ by **1H(H)**. In the same Scheme 1 is included also the possible formation of hydrogen peroxide as the result of direct elimination from the formed **1H(OOH)** complex and, as a consequence, the pathway for the reaction of the released H₂O₂ with **1H(H)** to give the restored catalyst and water. Formation of hydrogen peroxide was not observed via ¹H NMR, and this is why Heiden and Rauchfuss did not take into consideration this hypothesis,⁶ envisaged instead by Ikariya and co-workers.⁵

In this paper, our goal is to investigate by density functional theory (DFT) the mechanistic details of the overall reaction of

- (5) Arita, S.; Koike, T.; Kayaki, Y.; Ikariya, T. *Angew. Chem., Int. Ed.* **2008**, *47*, 2447–9.
- (6) Heiden, Z. M.; Rauchfuss, T. B. *J. Am. Chem. Soc.* **2007**, *129*, 14303–14310.
- (7) (a) Bahrke, T.; Lenz, O.; Krauss, N.; Friedrich, B. *J. Biol. Chem.* **2005**, *280*, 23791–23796. (b) Kanai, R.; Miyachi, S.; Takamiya, A. *Nature* **1960**, *188*, 873–875.

- (8) (a) Wick, D. D.; Goldberg, K. I. *J. Am. Chem. Soc.* **1999**, *121*, 11900–11901. (b) Thyagarajan, S.; Incarvito, C. D.; Rheingold, A. L.; Theopolis, K. H. *Chem. Commun.* **2001**, 2198–2199. (c) Denney, M. C.; Smythe, N. A.; Cetto, K. L.; Kemp, R. A.; Goldberg, K. I. *J. Am. Chem. Soc.* **2006**, *128*, 2508–2509. (d) James, B. R.; Morris, R. H.; Kvintorics, P. *Can. J. Chem.* **1986**, *64*, 897–903.
- (9) (a) Keith, J. M.; Muller, R. P.; Kemp, R. A.; Goldberg, K. I.; Goddard, W. A., III. *J. Inorg. Chem.* **2006**, *45*, 9631–9633. (b) Chowdhury, S.; Rivalta, I.; Russo, N.; Sicilia, E. *Chem. Phys. Lett.* **2007**, *443*, 183–189.
- (10) Konnick, M. M.; Gandhi, B. A.; Guzei, I. A.; Stahl, S. S. *Angew. Chem., Int. Ed.* **2006**, *45*, 2904–2907.
- (11) (a) Popp, B. V.; Stahl, S. S. *J. Am. Chem. Soc.* **2007**, *129*, 4410–4422. (b) Chowdhury, S.; Rivalta, I.; Russo, N.; Sicilia, E. *J. Chem. Theory Comput.* **2008**, *4*, 1283–1292.

the iridium transfer hydrogenation catalyst $\text{Cp}^*\text{Ir}(\text{TsDPEN-H})$ with H_2 and O_2 with the support of the experimental observations and the proposed reaction mechanism. In addition, some preliminary calculated results are presented concerning the mechanism and the energetics of the O_2 activation process in acidic conditions, which was not experimentally investigated and should significantly differ with respect to the mechanism in neutral conditions. The first step of the work concerns the hydrogenation mechanism of both neutral **1** and protonated $[\text{IH}]^+$ complexes. Since very few studies^{2,12} were reported so far about the theoretical investigation of hydrogen transfer homogeneous catalytic systems and none of them concern the use of such compounds as catalysts for oxygen reduction, we guess this work could contribute to enhance further understanding and provide helpful information that would inspire the design of new catalysts for fuel cells.

To date, it is still a difficult challenge to obtain experimentally direct and accurate insight in the mechanistic pathways of chemical reactions. The most important limitation is the fact that key intermediates often have a very short lifetime. Obviously this holds also for the transition metal catalyzed reactions of the type addressed in the present paper. Computational studies do not suffer from these limitations and provide therefore a valuable complementary approach to study these reactions.

2. Computational Details

All molecular geometries were optimized at the Becke3-LYP (B3LYP) level of density functional theory.^{13,14} Frequency calculations at the same level of theory were also performed to identify all stationary points as minima (zero imaginary frequencies) or transition states (one imaginary frequency). The transition states involved were checked by IRC (intrinsic reaction coordinate) analysis.^{15,16} The effective core potentials (ECPS) of Hay and Wadt with double- ζ valence basis sets (LanL2DZ)¹⁷ were used to describe the iridium atom, while the standard 6-31G** basis sets of Pople and co-workers were used for the rest of the atoms. Final energies were calculated by performing single-point calculations on the optimized geometries at the same level of theory and employing 6-311+G(2d,2p) standard basis sets for H, C, O, and S atoms. No significant difference between the description of the calculated pathways in terms of total energy changes and enthalpy changes exists. Therefore, only total energies are reported and discussed. All the calculations were performed with the GAUSSIAN-03 software package.¹⁸

In order to reduce the computational cost, the methyl groups of the Cp^* ligand were substituted with hydrogen atoms. For this reason, from now we will indicate the simplified models of the studied complexes as $\text{CpIrH}(\text{TsDPEN})$ (**1**) and $\text{CpIr}(\text{TsDPEN-H})$

- (12) (a) Alonso, D. A.; Brandt, P.; Nordin, S. J. M.; Andersson, P. G. *J. Am. Chem. Soc.* **1999**, *121*, 9580–9588. (b) Petra, D. G. I.; Reek, J. N. H.; Handgraaf, J. W.; Meijer, E. J.; Dierkes, P.; Kamer, P. C. J.; Brussee, J.; Schoemaker, H. E.; van Leeuwen, P. W. N. M. *Chem.—Eur. J.* **2000**, *6*, 2818–2829. (c) Yamakawa, M.; Ito, H.; Noyori, R. *J. Am. Chem. Soc.* **2000**, *122*, 1466–1478. (d) Noyori, R.; Yamakawa, M.; Hashiguchi, S. *J. Org. Chem.* **2001**, *66*, 7931–7944. (e) Abdur-Rashid, K.; Clapham, S. E.; Hadzovic, A.; Lough, A. J.; Morris, R. H. *J. Am. Chem. Soc.* **2002**, *124*, 15104–15118. (f) Handgraaf, J. W.; Reek, J. N. H.; Meijer, E. J. *Organometallics* **2003**, *22*, 3150–3157. (g) Siwei Bi, S.; Xie, Q.; Zhao, X.; Zhao, Y.; Kong, X. *J. Org. Chem.* **2008**, *69*, 633–638.
- (13) Becke, A. D. *J. Chem. Phys.* **1993**, *98*, 5648–5652.
- (14) Stephens, P. J.; Devlin, F. J.; Chabalowski, C. F.; Frisch, M. J. *J. Phys. Chem.* **1994**, *98*, 11623–11627.
- (15) Fukui, K. *J. Phys. Chem.* **1970**, *74*, 4161–4163.
- (16) Gonzalez, C.; Schlegel, H. B. *J. Chem. Phys.* **1989**, *90*, 2154–2161.
- (17) Hay, P. J.; Wadt, W. R. *J. Chem. Phys.* **1985**, *82*, 299–311.
- (18) Frisch, M. J.; et al. *Gaussian03, Revision B.04*; Gaussian, Inc.: Pittsburgh, PA, 2003.

(**1H(H)**). In addition, the computational effort required to investigate the last part of the process, that is, the elimination of water from the iridium hydroperoxide complex by reaction with **1H(H)** to restore the **1** catalyst, was reduced replacing all the phenyl groups of the TsDPEN ligand with less demanding methyl groups.

Along the pathway for the insertion of triplet molecular oxygen into the metal–hydride bond both triplet and singlet multiplicities were examined for all the involved species. $\langle S^2 \rangle$ values were checked to assess whether spin contamination can influence the quality of the results. For triplet-state structures no significant contamination was found by unrestricted calculations. On the other hand, a $\langle S^2 \rangle$ value close to 1.0 for two singlet-state structures, besides molecular singlet oxygen, indicated a contamination by the triplet spin. The method proposed by Ovchinnikov and Labanowski¹⁹ was used for correcting the mixed spin energies and removing the foreign spin components. For molecular oxygen, for example, due to the contamination of the singlet wave function with the triplet state, a highly stable singlet ${}^1\Delta_g$ state was obtained corresponding to an excitation energy of 10.5 kcal/mol. Adopting the mentioned correction scheme, the triplet–singlet energy gap of O_2 was calculated to be 20.7 kcal/mol, which is in good agreement with the experimental value.²⁰

The impact of solvation effects on the energy profiles was estimated by using Tomasi's implicit polarizable continuum model (PCM)²¹ as implemented in Gaussian03. The Pauling set of radii was used to build up the cavity. Since preliminary calculations clearly showed that geometry relaxation effects are not significant, the solvation Gibbs free energies were calculated in implicit acetonitrile ($\epsilon = 36.64$) with the above method, performing single-point calculations on all stationary point structures obtained from vacuum calculations. Reaction Gibbs free energies in solution, ΔG_{sol} , were calculated for each process as the sum of two contributions: a gas-phase reaction free energy, ΔG_{gas} , and a solvation reaction free energy term calculated with the continuum approach, ΔG_{solv} .

The seam-search method of Harvey and co-workers²² was used to locate the minimum energy crossing point (MECP) between the triplet surface of reactants and the singlet one of the products along the oxygenation pathway of the Ir-hydride complex. Minimum energy crossing point (MECP) calculations were carried out using Gaussian 98 (G98)²³ with optimization criteria approximately 3 times larger than the default values used within G03.

NBO charge analysis was carried out on the structures of some intercepted stationary points.²⁴

3. Results and Discussion

3.1. Hydrogenation Reaction. In this section the results of the investigation of the reaction mechanism for the addition of H_2 to complex **1** to give the amine hydride $\text{Cp}^*\text{IrH}(\text{TsDPEN})$ (**1H(H)**) are given. Since it was reported that the reaction is accelerated by Brønsted acids, which convert **1** into the unsaturated iridium(III) amine cation $[\text{Cp}^*\text{Ir}(\text{TsDPEN})]^+$ ($[\text{IH}]^+$),^{3,25} the pathways for the addition of molecular hydrogen

- (19) Ovchinnikov, A. A.; Labanowski, J. K. *Phys. Rev. A* **1996**, *53*, 3946–3952.
- (20) Weissbluth, M. *Atoms and Molecules*; Academic Press: New York, 1978; p 587.
- (21) (a) Miertus, S.; Scrocco, E.; Tomasi, J. *Chem. Phys.* **1981**, *55*, 117–129. (b) Miertus, S.; Tomasi, J. *Chem. Phys.* **1982**, *65*, 239–245.
- (22) Harvey, J. N.; Aschi, M.; Schwarz, H.; Koch, W. *Theor. Chem. Acc.* **1998**, *99*, 95–99.
- (23) Frisch, M. J.; et al. *Gaussian 98, Revision A.9*; Gaussian, Inc.: Pittsburgh, PA, 2001.
- (24) (a) Carpenter, J. E.; Weinhold, F. J. *Mol. Struct.* **1988**, *169*, 41. (b) Carpenter, J. E.; Weinhold, F. J. *The Structure of Small Molecules and Ions*; Plenum: New York, 1988.
- (25) Heiden, Z. M.; Rauchfuss, T. B. *J. Am. Chem. Soc.* **2009**, *131*, 3539–3600.

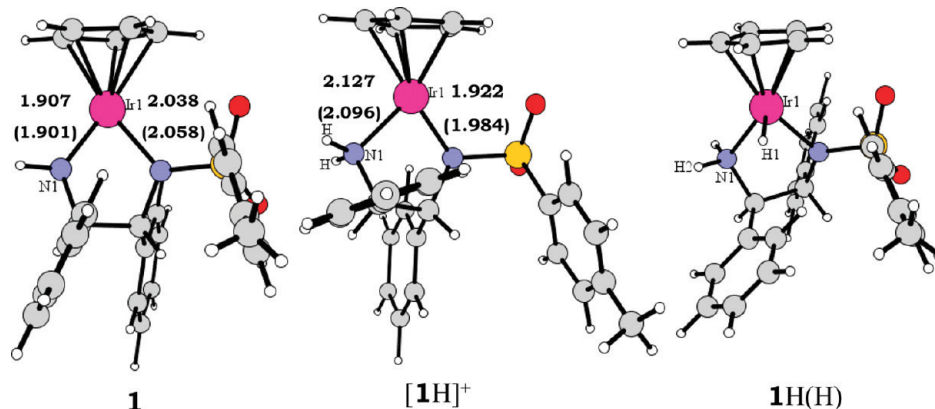


Figure 1. Fully optimized structures of the reference **1** and $[1\text{H}]^+$ and hydrogenated amine hydride **1H(H)** complexes. Selected bond lengths (in Å) are compared with available experimental values (in parentheses).

to both **1** and $[1\text{H}]^+$ complexes were investigated. The ground-state optimized structures of the reference complexes **1** and $[1\text{H}]^+$ chosen as the starting point for our study are shown in Figure 1 along with the optimized structure of the hydrogenated amine hydride complex **1H(H)**. Comparison with the most relevant available experimental structural features^{26,27} for complexes **1** and $[1\text{H}]^+$ shows a good agreement, indicating the modeling of the catalysts is good. The confirmed elongation by about 0.2 Å of the Ir–NH bond and the shortening by about 0.1 Å of the Ir–NTs bond caused by protonation of **1** are indicative that protonation redirects π -bonding from one nitrogen to the other.

For the hydride **1H(H)** the conformer with the phenyl groups in equatorial position with respect to the IrN_2C_2 ring is only slightly more stable than the conformer with the two phenyl groups axially oriented, with the calculated difference in gas phase being less than 1 kcal/mol. Some additional information on the fully optimized geometrical structures of these complexes can be found in the Supporting Information, Tables S1 and S2.

3.1.1. Addition of H₂ to the CpIr(TsDPEN-H) Neutral System. The calculated B3LYP PES for the hydrogenation process of **1** is drawn in Figure 2, where relative energies in gas phase and relative free energies in solution are calculated with respect to the ground-state reactants' asymptote (**1** + H₂).

Optimized structures of intermediates and transition states intercepted along the hydrogenation pathway are shown in the same figure, whereas selected geometric parameters for stationary points are reported in Table S1 of the Supporting Information.

The interaction of the hydrogen molecule with complex **1**, as the first step of the mechanism, leads to the formation of a very weakly bound van der Waals complex, **1**·H₂, that is slightly less stable than reactants both in gas phase (1 kcal/mol) and in solution (3 kcal/mol). It is well known²⁸ that weak van der Waals interactions are inadequately described using standard functionals such as B3LYP. Therefore, although van der Waals complexes do not play any key role in the present context, it is worthy to underline that the energetics of such species could not be accurately calculated, and even their presence along the

reaction pathway could be the result of the employed computational protocol.

The next step, which is the rate-determining one, involves coordination of dihydrogen to the metal center. As a result, an intermediate, **1HH**, is formed, which lies 16.0 kcal/mol higher in energy with respect to reactants. The transition state, TS1, that it is necessary to surmount to form the **1HH** intermediate lies 27.3 kcal/mol (24.6 kcal/mol in solvent) above the reactants' energy and is characterized by an imaginary frequency calculated to be 477*i* cm⁻¹, associated with the breaking of the H–H bond and formation of the new Ir–H bonds. Formation of the final hydrogenated product, **1H(H)**, takes place, overcoming an energy barrier of 13.1 and 14.7 kcal/mol in gas phase and solvent, respectively, corresponding to the TS2 transition state. The normal mode associated with the imaginary frequency, calculated to be 1089*i* cm⁻¹, corresponds to the transfer of a hydrogen atom from Ir to the N atom of the amide. The overall conversion reaction of **1** to **1H(H)** is exothermic by 9.7 kcal/mol in gas phase and 12.5 kcal/mol in solvent.

3.1.2. Addition of H₂ to the [CpIr(TsDPEN)]⁺ Cationic System. The calculated potential energy surface for the H₂ addition to the unsaturated iridium(III) amine cation CpIr(TsDPEN)⁺ ($[1\text{H}]^+$) is depicted in Figure 3. Structures of stationary points are reported along the pathway, while geometrical information is reported in the Supporting Information (see Table S2). As pointed out by Heiden and Rauchfuss,²⁷ the rate of the proton-catalyzed addition of H₂ to **1** varies over 3 orders of magnitude depending on the acid.

The proposed mechanism involves protonation of the NH center in the five-coordinate diamide to give the amido-amine complex $[1\text{H}]^+$ followed by formation of the corresponding dihydrogen complex $[1\text{H}(\text{H}_2)]^+$ by hydrogen addition.

The propagation of the cycle is guaranteed by the possibility of the dihydrogen complex to protonate the parent diamido **1**, either directly or via a more efficient anion-assisted proton transfer. The authors demonstrated also that the proton that is transferred is derived from the dihydrogen ligand. According to this hypothesis, the first step we considered is the formation of a weakly bound ion–molecule complex, $[1\text{H}\cdot\text{H}_2]^+$, which is destabilized by 3.2 kcal/mol in solvent (1.3 kcal/mol in gas phase) with respect to reactants. The acid-catalyzed addition of hydrogen to the diamido complex **1** proceeds with the formation of the dihydrogen complex $[1\text{H}(\text{H}_2)]^+$, which takes place overcoming a free energy barrier of 9.6 kcal/mol in solution, corresponding to the transition state TS1⁺. The imaginary

- (26) Heiden, Z. M.; Gorecki, B. J.; Rauchfuss, T. B. *Organometallics* **2008**, *27*, 1542–1549.
- (27) Heiden, Z. M.; Rauchfuss, T. B. *J. Am. Chem. Soc.* **2006**, *128*, 13048–13049.
- (28) Vincent, M. A.; Hillier, I. H.; Morgado, C. A.; Burton, N. A.; Shan, X. *J. Chem. Phys.* **2008**, *128*, 44313–44320, and references therein.

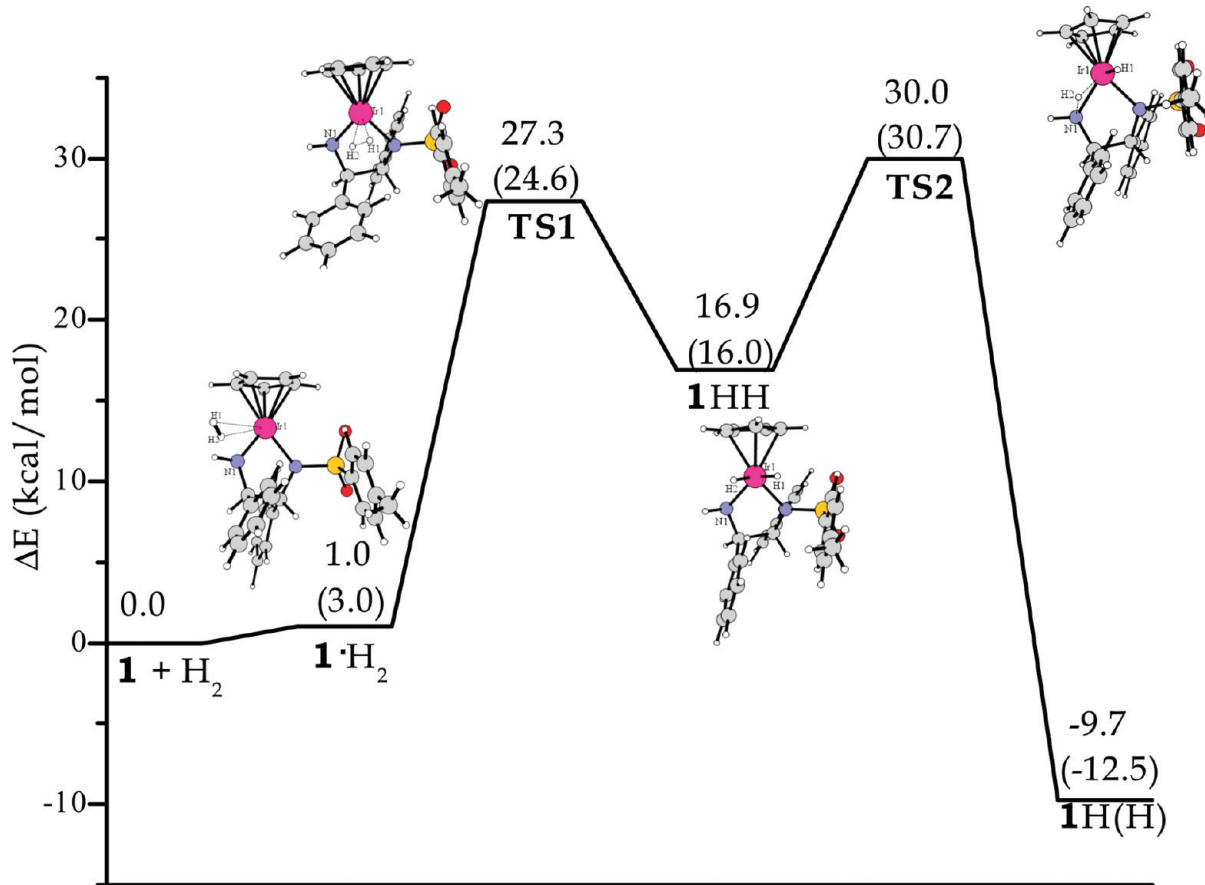


Figure 2. Calculated B3LYP PES for the hydrogenation reaction of CpIr(TsDPEN-H). Gibbs free energy changes at 298.15 K in CH₃CN are also reported in parentheses. Energies are in kcal/mol and relative to ground-state reactants.

frequency that confirms the nature of this stationary point is calculated to be 299*i* cm⁻¹ and corresponds to the movement of molecular hydrogen coming close the metal center. The [1H(H₂)]⁺ complex is formed, in which the H1–H2 bond length is stretched from 0.743 Å to 0.841 Å as a consequence of coordination. Along the reaction pathway we intercepted a second transition state, TS2⁺, that is necessary to surmount to form a third intermediate, [1H(HH)]⁺, in which the H1–H2 bond is definitely broken and two new metal–hydride bonds are formed. The activation barrier is only 2.1 kcal/mol in acetonitrile, and the imaginary frequency is 798.9*i* cm⁻¹.

The final product, that is, the hydrogenated amine hydride complex **1H(H)**, is obtained by deprotonation of [1H(HH)]⁺. Since the calculation of the anion-assisted deprotonation pathway is obviously less computationally demanding than deprotonation by direct reaction with **1**, we have investigated the PES for the deprotonation assisted by the anion of the triflic acid (OTf⁻). The details of our computational analysis concerning this last part of the hydrogenation process (dashed line in Figure 3) are reported in Figure 4. According to experimental findings, the anion does not appear to be coordinated to the metals center of the [1H]⁺ charged complex and is hydrogen-bonded to the axial amine proton (Supporting Information, Table S3). As expected, the calculated O–H bond length is significantly shorter than the value extracted from the crystallographic characterization of the salt (1.786 versus 2.048 Å).²⁶ Preliminary calculations clearly showed that no significant structural change is introduced by the presence of the bulky Cp* ligand. In Figure 4 are reported the structures of the two transition states, TS1OTf and TS2OTf, intercepted along the deprotonation pathway of

[1H(HH)]⁺ assisted by the OTf⁻ anion, which does not compete with the molecular oxygen for the coordination to the metal center.

The TS1OTf transition state is formed by surmounting a very low energy barrier (3.5 and 2.8 kcal/mol in gas phase and in solution, respectively). The normal mode associated with the imaginary frequency of 249*i* cm⁻¹ for this transition state corresponds to the shift of a proton from the Ir center to the oxygen atom of the anion. The TS2OTf structure, instead, lies very high in energy and is characterized by an imaginary frequency of 1097*i* cm⁻¹, corresponding to the concerted proton transfer from the iridium center to the amine nitrogen atom and from the nitrogen atom to the anion. This outcome confirms that the involved proton is derived from the dihydrogen ligand as experimentally hypothesized.

From a comparison of the complete hydrogenation pathways of the neutral CpIr(TsDPEN-H) and protonated CpIr(TsDPEN)⁺ complexes it results that the barriers that hamper the hydrogenation path are significantly lower when the molecular hydrogen addition is acid-catalyzed (see Figures 2, 3, and 4).

3.2. Insertion of O₂ into the Ir–H Bond. Singlet and triplet calculated B3LYP PESs for the oxygenation process of **1H(H)** are drawn in Figure 5. In the same figure, along the oxygenation pathway, are sketched the structures of stationary points, except the ground-state singlet structure of the hydroperoxo complex, which is reported in Figure 6 together with the calculated MECP. Selected geometrical parameters can be found in the Supporting Information (see Tables S4 and S5). Relative energies in gas phase and relative free energies in CH₃CN have been calculated with respect to the ground-state reactants' asymptote **1H(H)** +

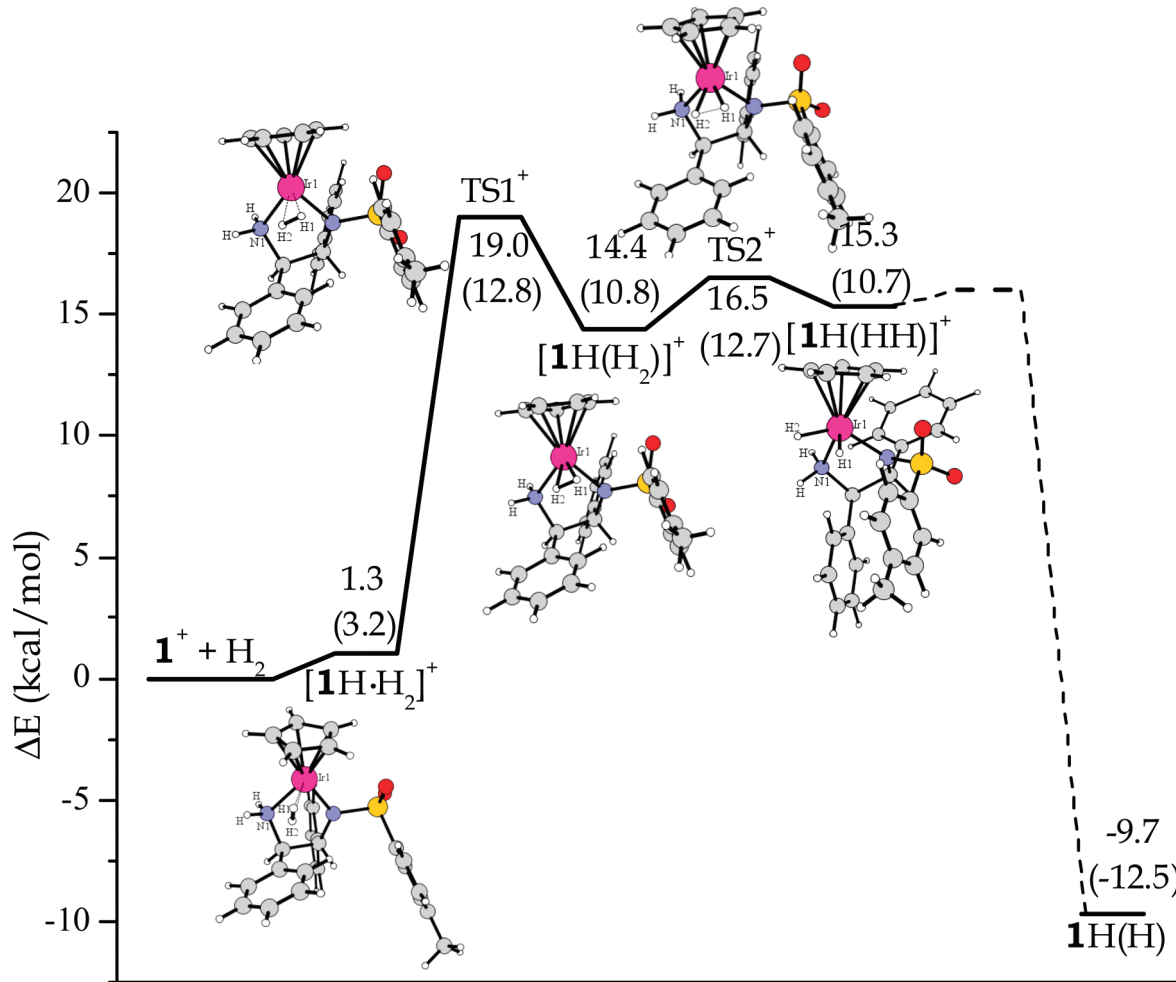


Figure 3. Calculated B3LYP PES for the hydrogenation reaction of $[\text{CpIr}(\text{TsDPEN})]^+$. Gibbs free energy changes at 298.15 K in CH_3CN are also reported in parentheses. Energies are in kcal/mol and relative to ground-state reactants.

$^3\text{O}_2$. As illustrated in the next paragraphs, the molecular oxygen addition to the Ir center follows the same path described in our previous detailed computational studies of the mechanism of such a process.^{9b,11b} The addition of triplet molecular oxygen leads to the formation of a weakly bound van der Waals adduct, $\mathbf{1}\mathbf{H}(\mathbf{H})\cdot\mathbf{O}_2(3)$, whose formation is slightly endothermic in solution ($\Delta E = 1.6$ kcal/mol). The optimized structure of the corresponding complex in a singlet state, $\mathbf{1}\mathbf{H}(\mathbf{H})\cdot\mathbf{O}_2(1)$, is substantially different since in this case O_2 appears to be directly coordinating to the metal center. It lies at 14.9 and 17.3 kcal/mol above the entrance channel of the separated reactants in gas phase and in solvent, respectively. The reported energy for this adduct was properly corrected using the above-mentioned scheme,¹⁹ since calculations showed significant triplet spin contamination.

The next step of the process involves the abstraction of the hydrogen atom from the iridium center by O_2 . Along the triplet pathway the activation barrier of 9.3 kcal/mol in acetonitrile (14.4 kcal/mol in gas phase) that needs to be overcome corresponds to the formation of the $\mathbf{TS3}(3)$ transition state. The Ir–H1 bond distance lengthens from 1.574 to 1.685 Å and the O–O bond length stretches from 1.254 to 1.346 Å. The calculated O–H distance is 1.518 Å, indicating that the $\text{O}_2\text{–H1}$ bond is forming. The imaginary frequency, calculated to be 667i cm^{-1} , corresponds to the movement of the hydrogen atom detaching from Ir and bonding to oxygen. As a result, an

intermediate is formed, $\mathbf{1}\mathbf{H}(\text{HOO})$, that lies 2.3 kcal/mol below the $\mathbf{TS3}(3)$ in solution, in which the peroxyl HOO radical is coordinating with the metal center of the complex through a weak interaction between Ir and hydrogen atoms.

On the other hand, along the singlet pathway a transition state, $\mathbf{TS3}(1)$, is intercepted and characterized where the closest oxygen and hydrogen distance is 1.505 Å. Also for this transition state, which lies 26.0 kcal/mol above the reactants' dissociation limit in solution, the absolute energy was corrected for spin contamination. The reaction proceeds with the formation of an intermediate, $\mathbf{1}\mathbf{H}(\text{OHO})$, whose formation is exothermic by 6.0 kcal/mol in CH_3CN . The significant feature of this intermediate, in analogy with previous theoretical results,^{9b,11b} is that the hydrogen atom is bonded to the proximal oxygen, whereas the distal oxygen atom is rotated upward. Since the singlet structure of the $\mathbf{1}\mathbf{H}(\text{OHO})$ complex is more stable than the $\mathbf{1}\mathbf{H}(\text{OOH})$ triplet intermediate, in this region of the PES a spin inversion has to occur after the passage of the $\mathbf{TS3}(3)$ transition state. In the framework of the two-state reactivity (TSR) paradigm, this kind of spin crossing occurring after formation of the transition state cannot be considered a rate-limiting factor.²⁹ By using the method mentioned above, the MECP between the triplet and singlet surfaces has been individuated, and the structure at this

(29) Schröder, D.; Shaik, S.; Schwarz, H. *Acc. Chem. Res.* **2000**, *33*, 139–145.

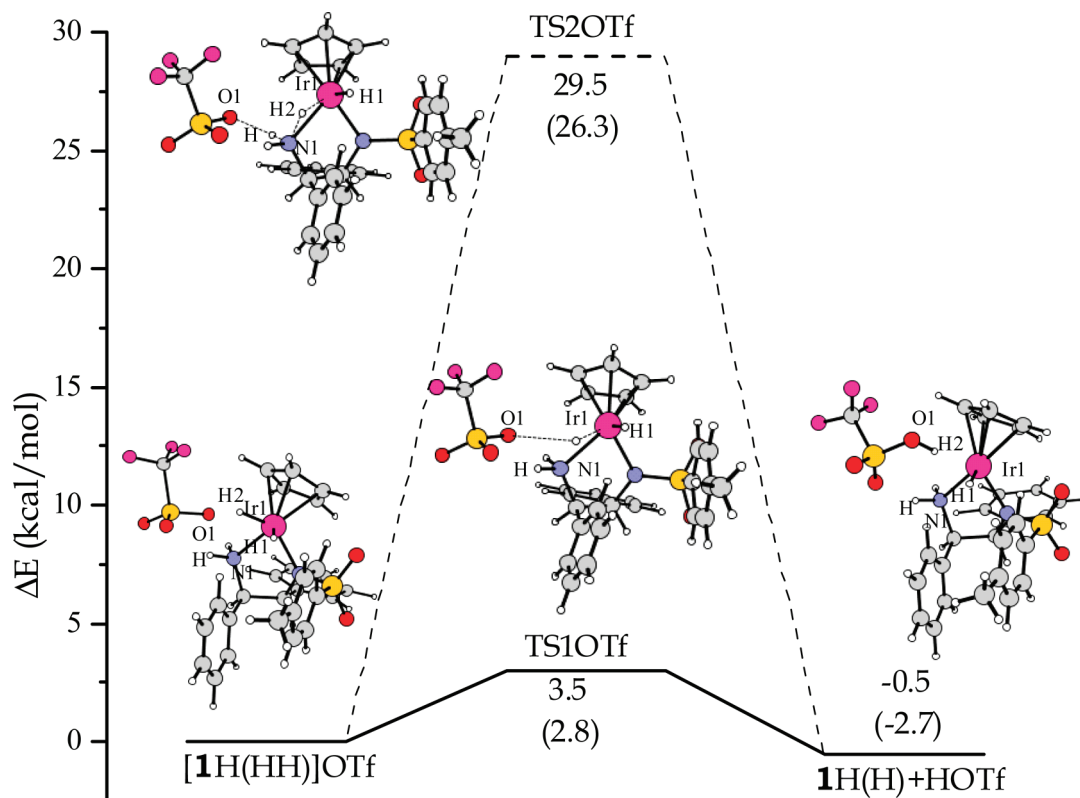


Figure 4. Calculated energy changes (in kcal/mol) for the deprotonation reaction of the hydrogenated amido-amine cation $[1\text{H}(\text{HH})]^+$ assisted by the OTf^- anion, both in gas phase and in solution (in parentheses).

point exhibits a geometry very similar to the $1\text{H}(\text{OHO})$ singlet intermediate. Crossing point relative energy calculated in gas phase and solution is reported in Figure 5.

After the crossing the reaction proceeds along the singlet path with the formation of the final Ir-hydroperoxo complex, and the overall process is calculated to be exothermic by 23.9 kcal/mol in CH_3CN solvent and 15 kcal/mol in gas phase. The reaction evolves through the breaking of the bond between the proximal oxygen and the Ir center, which makes a new bond with the distal oxygen. Triplet hydroperoxide product formation involves, instead, rearrangement of the HOO fragment in such a way that terminal oxygen and hydrogen atoms move in opposite directions toward and away from the Ir center, respectively. Both of the corresponding transition states, $\text{TS4}(1)$ and $\text{TS4}(3)$, have been intercepted and confirmed by IRC analysis. The singlet $\text{TS4}(1)$ structure lies 19.9 kcal/mol–17.3 kcal/mol when solvent effects are included—above the reactants’ dissociation limit and is characterized by an imaginary frequency of $340\text{i}\text{ cm}^{-1}$. Along the triplet PES the $\text{TS4}(3)$ structure is destabilized with respect to reactants by 23.9 kcal/mol in gas phase and by 20.7 kcal/mol in acetonitrile, and the corresponding imaginary frequency is calculated to be $255\text{i}\text{ cm}^{-1}$. Compared to the exothermic formation of the hydroperoxide product in its singlet multiplicity, the overall conversion process of the iridium hydride to the Ir-OOH species, $1\text{H}(\text{OOH})$, along the spin-conserving triplet surface is endothermic by 10.8 kcal/mol in gas phase and 8.8 kcal/mol in solvent.

The NBO charge analysis that was carried out on some stationary points intercepted along the O_2 reduction pathway gives some hints on the factors that could accelerate the process. Indeed, NBO analysis reveals that the hydride ligand in $1\text{H}(\text{H})$ bears a small positive charge of 0.090. As dioxygen approaches,

the hydride ligand acquires increasingly protic character (a charge of 0.106 for the first adduct), and at the transition state it has a positive charge of 0.238. The presence of ligands that possess greater electron-donating ability increases the hydridic character of the metal hydride and should facilitate the reduction of molecular oxygen. The presence of more electron-donating ligands also affects the basicity of the amine and should lead to an overall improved catalytic performance.

3.3. Mechanism for H_2O_2 Formation. Before examining the last step of the process that through water elimination regenerates complex **1**, the results of the computation of the pathway leading to the release of H_2O_2 from the hydroperoxide complex are illustrated. The B3LYP calculated PES for this process reported in Figure 7 shows the intramolecular amine hydrogen transfer to the hydroperoxide oxygen coordinated to the metal.

Selected geometrical parameters of stationary points can be found in Table S6 of the Supporting Information. The calculated energy barrier for this rearrangement is 12.5 kcal/mol in gas phase and 17.1 kcal/mol in solvent with respect to hydroperoxide complex. The imaginary frequency that confirms the nature of this stationary point is $578\text{i}\text{ cm}^{-1}$ and corresponds to the shift of one of the amine hydrogen atoms from nitrogen to oxygen to form a H_2O_2 molecule and regenerate catalyst **1**. Formation of products is calculated to be slightly exothermic (-1.8 kcal/mol in gas phase and -1.6 in acetonitrile) with respect to reactant $1\text{H}(\text{OOH})$.

Let us calculate the energetics of the H_2O_2 release reaction with respect to ground-state $1\text{H}(\text{H}) + {}^3\text{O}_2$ reactants. Since the singlet $1\text{H}(\text{OOH})$ intermediate in gas phase is stabilized by 15.0 kcal/mol (23.9 kcal/mol in solvent), the overall process for the H_2O_2 elimination appears to be exothermic by 16.8 kcal/mol (25.5 kcal/mol in solvent). The transition TS6 state lies at -2.5

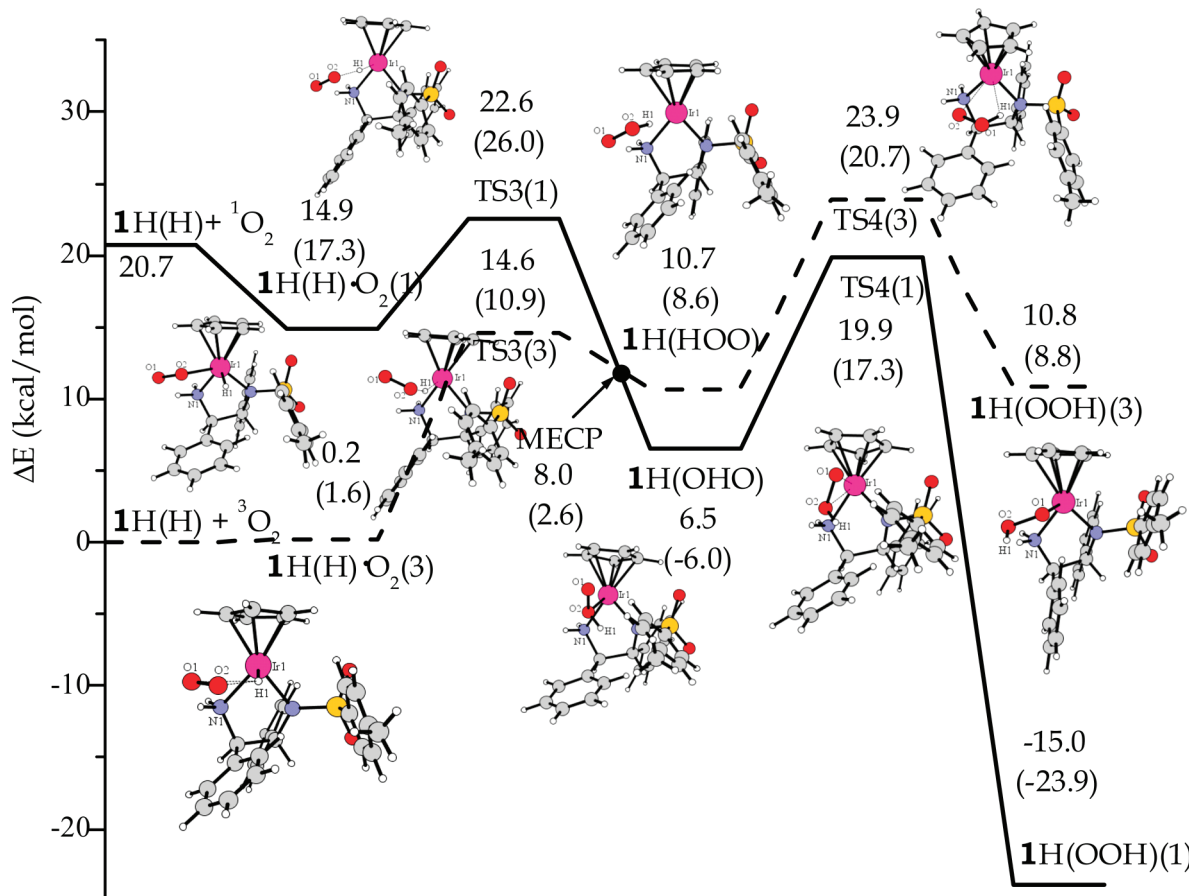


Figure 5. Singlet and triplet calculated B3LYP PESs for the oxygenation process of **1H(H)**. Gibbs free energy changes at 298.15 K in CH₃CN are also reported in parentheses. Energies are in kcal/mol and relative to **1H(H)** + ${}^3\text{O}_2$ ground-state reactants.

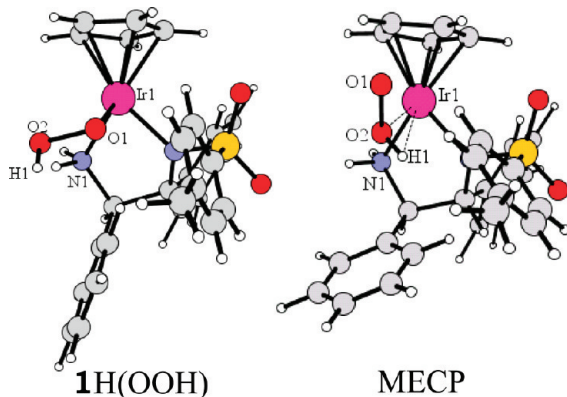


Figure 6. Fully optimized structures of the **1H(OOH)** hydroperoxo intermediate and minimum energy crossing point.

kcal/mol in gas phase (-6.8 kcal/mol in solvent) below the energy of **1H(H)** + ${}^3\text{O}_2$ separated reactants. Therefore, the H₂O₂ elimination process appears to be viable. In the next sections the outcomes of our computational analysis will be illustrated for both the hypothesized reaction mechanism that involves regeneration of **1** by reduction of **1H(OOH)** with **1(H)H** and the possibility that H₂O₂ reacts with **1(H)H** to provide **1** and water.

3.4. Mechanism for the Elimination of H₂O from **1H(OOH) by Reduction with **1H(H)**.** In this section the outcomes of our computational analysis concerning the last part of the overall **1H(H)** + O₂ process are presented, that is, elimination of water

to restore **1**, which is ready to be reduced by H₂. As underlined above, to make computations more tractable, phenyl groups of the TsDPEN ligand were replaced by methyl groups.

On the basis of several experimental indications, such as the second-order dependence of the reaction rate on the concentration of **1H(H)**, Heiden and Rauchfuss⁵ assumed that the formed hydroperoxo complex, **1H(OOH)**, is reduced by **1H(H)** to yield the corresponding hydroxy-amine, **1H(OH)**, which would eliminate water to regenerate the metal hydride. Concerning the mechanism of formation of the hydroxy-amine and the subsequent elimination of water we considered three possibilities that are sketched in Scheme 2.

Both paths (a) and (b) involve formation of two hydroxy-amine complexes as products of the first step of the reaction between **1H(OOH)** and **1H(H)**, whereas path (c) takes into account the possibility that a first water molecule is eliminated through a concerted mechanism and a hydroxy-amine molecule is produced together with the restored catalyst **1**. The intramolecular elimination of a water molecule from each **1H(OH)** complex is the second step of the (b) and (c) elimination pathways, whereas the intermolecular elimination of two water molecules by means of a concerted mechanism occurs along path (a).

The outcomes of our computational analysis are summarized in Figure 8 and will be illustrated in the next paragraphs.

3.4.1. Elimination of Water Involving Formation of Two Hydroxy-Amine Complexes. The reduction of the hydroperoxo complex **1H(OOH)** by **1H(H)** to form two hydroxy-amine complexes represents the first step of the hypothesized (a) and

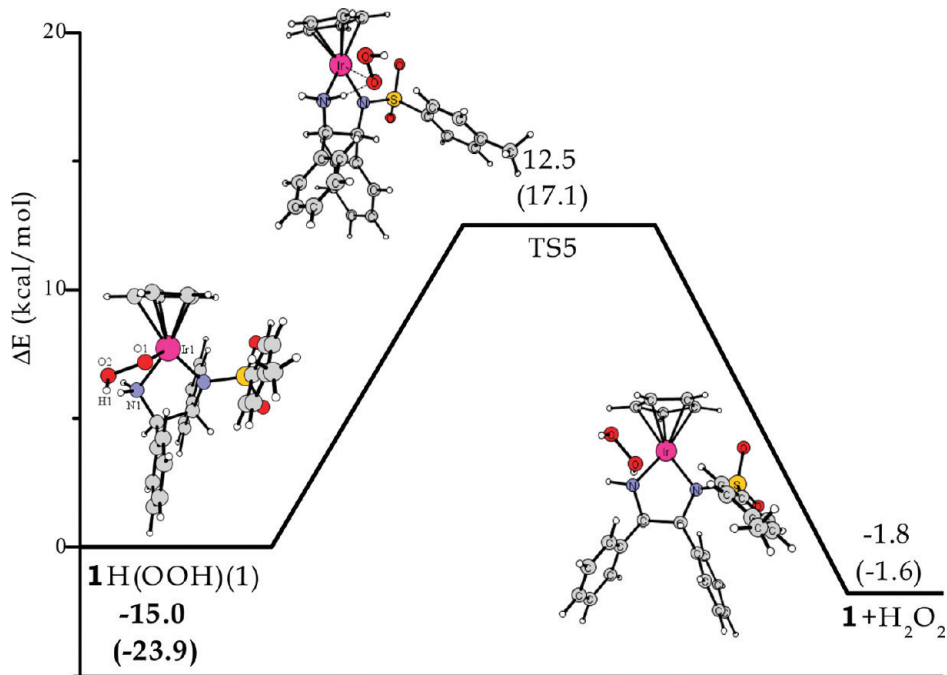
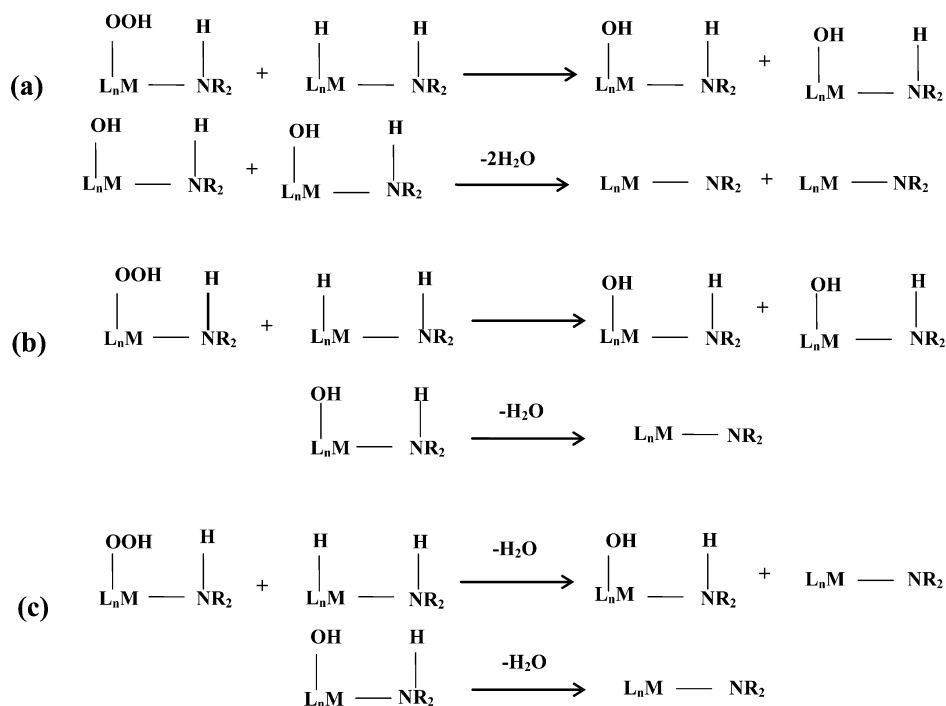


Figure 7. Calculated energy changes (in kcal/mol) for the H_2O_2 elimination reaction from $\mathbf{1}\text{H}(\text{OOH})$. The reference relative energy values (in bold and italicics) of the hydroperoxide formation with respect to the $\mathbf{1}\text{H}(\text{H}) + {}^3\text{O}_2$ ground-state reactants are also reported. Gibbs free energy changes at 298.15 K in CH_3CN are also reported in parentheses.

Scheme 2. Examined Mechanisms for Hydroxy-Amine Formation and Water Elimination



(b) pathways. The corresponding calculated PES is reported in Figure 8 (solid line). In the same figure is reported the energy profile for the concerted intermolecular elimination of two water molecules, which represents the second step of the water elimination pathway along the (a) profile. Selected geometrical parameters of stationary points can be found in Table S7 of the Supporting Information.

The two complexes approach to form the transition state **TS6(a)**, which lies 8.6 kcal/mol in gas phase and 16.6 kcal/mol in solvent above the energy of reactants. The normal mode

associated with the imaginary frequency, calculated to be 669i cm^{-1} , corresponds to the concerted transfer of the hydride to the distal oxygen, lengthening of the peroxide O–O bond, and simultaneous shift of the hydrogen atom of the OH group to the proximal oxygen. The result of this rearrangement, as confirmed by the IRC analysis, is the formation of two hydroxy-amine complexes that are more stable with respect to reactants by 61.6 kcal/mol in acetonitrile (62.4 kcal/mol in gas phase). The subsequent intermolecular elimination of two water molecules occurs by formation of the **TS7(c)** transition state,

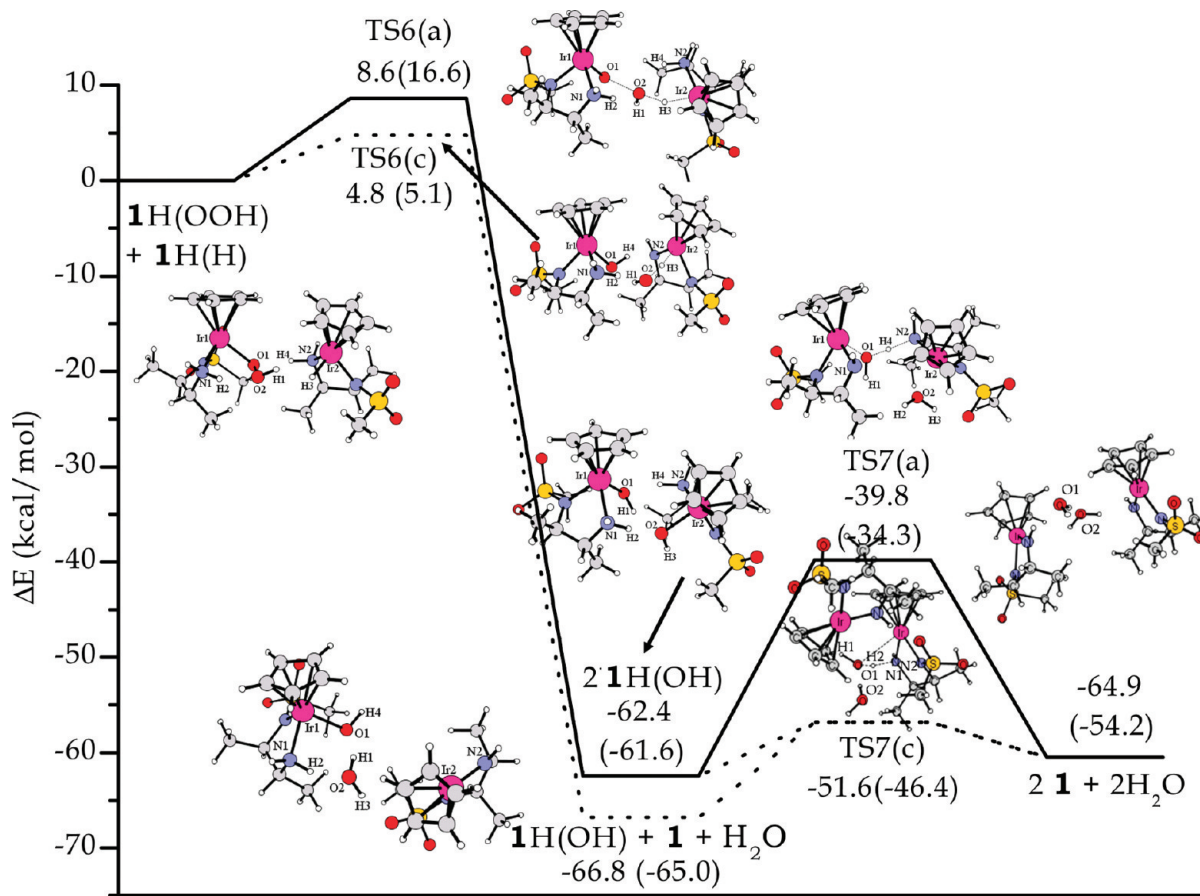


Figure 8. Calculated energy changes (in kcal/mol) for the hydroxy-amine formation and elimination of water, both in gas phase and in solution (in parentheses). The reaction between **1H(OOH)** and **1H(H)** involves at first formation of two hydroxy-amine complexes along pathways (a) and (b) (solid line), whereas path (c) (dotted line) takes into account the possibility that the first water molecule is eliminated through a concerted mechanism to form a hydroxy-amine molecule together with the restored catalyst **1**. The second step of the process is the intermolecular elimination of two water molecules by a concerted mechanism along path (a) and the intramolecular elimination of a water molecule from the **1H(OH)** complex along pathways (b) and (c).

overcoming an energy barrier of 22.6 and 27.3 kcal/mol in gas phase and in acetonitrile solvent, respectively. The normal mode associated with the calculated imaginary frequency of $92i\text{ cm}^{-1}$ corresponds to the simultaneous stretching of the Ir–O distances of both **1H(OH)** complexes and the transfer of one amine hydrogen atom of each molecule to the OH group of the other. The overall elimination process is calculated to be exothermic by 54.2 kcal/mol in solvent (64.9 kcal/mol in gas phase).

3.4.2. Stepwise Elimination of Two Water Molecules. The calculated energy profile for the pathway, named (c) in Scheme 2, which involves the elimination of two water molecules in two steps, is sketched in Figure 8 (dotted line). Selected geometrical parameters of involved stationary points are reported in Table S8 of the Supporting Information. The elimination of one water molecule in the first part of pathway (c) occurs by overcoming an energy barrier of 4.8 kcal/mol in gas phase and 5.1 kcal/mol in solvent for the TS6(c) transition state. The imaginary frequency that characterizes this transition state is $683i\text{ cm}^{-1}$. The products, catalysts **1** and hydroxy-amine complex together with a water molecule, are obtained by means of a concerted transfer of one amine hydrogen atom from the **1H(H)** complex to the proximal oxygen, stretching of the peroxide O–O bond, and a simultaneous shift of the hydride from complex **1H(H)** to the distal oxygen of the OOH moiety. The IRC analysis of the structures along the reaction coordinate from the TS7(c) transition state to the reactants and products confirms that TS7(c) is connected to both **1H(OOH)** and **1H(H)**

reactants and **1**, **1H(OH)**, and water products. The second step of the path, which coincides with the second step of pathway (b), is the elimination of a water molecule from the hydroxy-amine complex. The reaction occurs via a transition state named TS7(a), corresponding to the intramolecular amine hydrogen shift to the hydroxide oxygen atom. The calculated energy barrier for this rearrangement is 15.2 kcal/mol in gas phase and 18.6 kcal/mol in solvent. The single imaginary frequency for the four-membered transition state is $729i\text{ cm}^{-1}$ and describes the shift of one of the amine hydrogen atoms from nitrogen to oxygen to form a water molecule and regenerate the catalyst **1**.

From the comparison reported in Figure 8 of the energetics of the three hypothesized water elimination pathways, it appears that the most favorable pathway is that indicated as (c). To be precise, according to experimental predictions the reaction between complexes **1H(H)** and **1H(OOH)** produces **1**, H_2O , and **1H(OH)**. From the hydroxy-amine complex a second H_2O molecule is eliminated by an intramolecular hydrogen shift. The rate-determining step of the process is the elimination of the first water molecule, which requires an energy barrier in excess by 5.1 kcal/mol in solvent (4.8 in gas phase) with respect to reactants to be surmounted. The transition-state barrier for the elimination of the second water molecule, even if higher, lies well below the reactants' energy.

A comparison between the PESs reported in Figures 5 and 8 clearly shows that the barrier heights relative to the transition states intercepted along the water elimination pathways are low

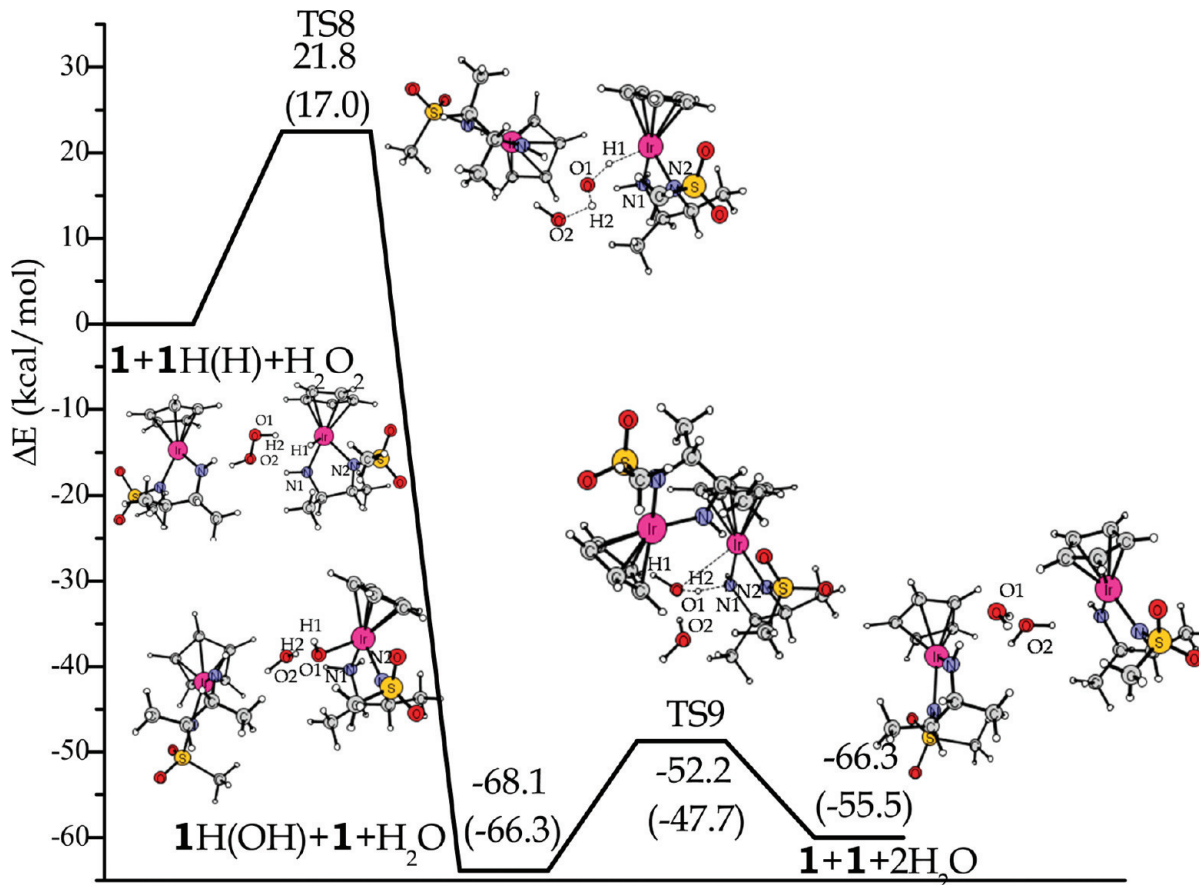


Figure 9. Calculated energy changes (in kcal/mol) for the H_2O elimination reaction by reduction of H_2O_2 with $\mathbf{1}\text{H}(\text{H})$. Gibbs free energy changes at 298.15 K in CH_3CN are also reported in parentheses.

and do not exceed the energy of the $\mathbf{1}\text{H}(\text{H}) + \text{O}_2$ ground-state reactants' asymptote. Therefore, the slow step of the whole hydrogenation process is the O_2 insertion into the Ir–H bond to produce the $\mathbf{1}\text{H}(\text{OOH})$ hydroperoxide complex hampered, besides the triplet to singlet crossing, by rather high barriers. In particular, the energy barrier for the rearrangement of the OOH fragment to yield the hydroperoxo product along the singlet path was calculated to be 19.9 kcal/mol in gas phase and 17.3 kcal/mol in acetonitrile solvent, which well reproduces the value experimentally estimated (18.9 kcal/mol).⁵ The unreacted $\mathbf{1}\text{H}(\text{H})$, therefore, approaches formed $\mathbf{1}\text{H}(\text{OOH})$, where the reaction occurs by deprotonation of the NH_2 group and hydride transfer, to result in $\mathbf{1}\text{H}(\text{OH})$ formation.

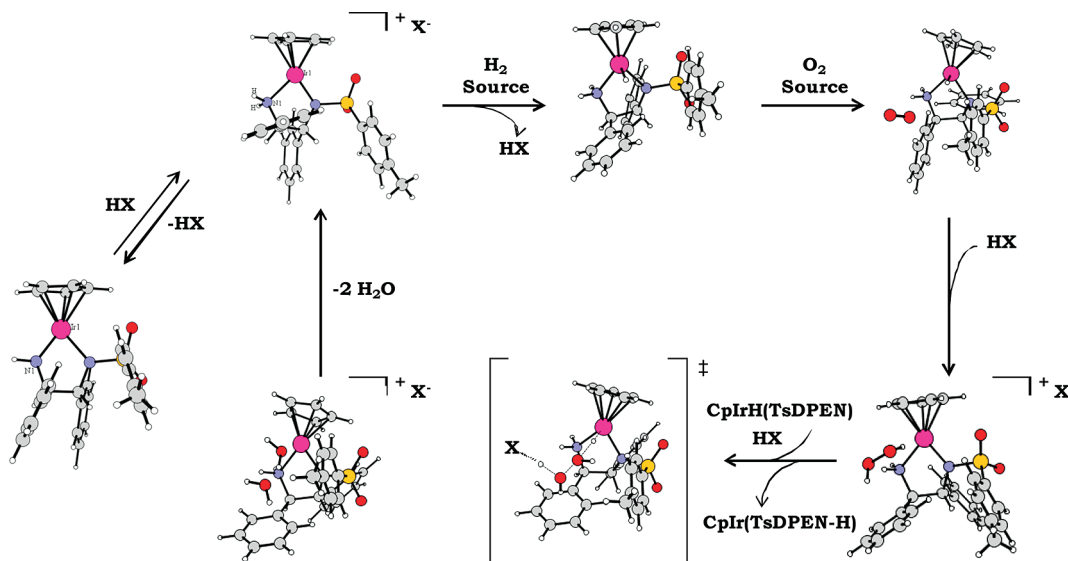
3.5. Mechanism for the Elimination of H_2O from H_2O_2 by Reduction with $\mathbf{1}\text{H}(\text{H})$. As stated above, if the hypothesis that H_2O_2 is released from the $\mathbf{1}\text{H}(\text{OOH})$ complex is taken into account, the final step of the whole process should be the elimination of water by reaction between the hydrogen peroxide product and $\mathbf{1}\text{H}(\text{H})$, consistent with the observed second-order kinetics. The B3LYP calculated PES reported in Figure 9 shows the outcomes of our computational analysis. As H_2O_2 comes close to the $\mathbf{1}\text{H}(\text{H})$ complex, the transition state TS8 is formed, which lies 21.8 kcal/mol in gas phase and 17.0 kcal/mol in solvent above the energy of reactants. The normal mode associated with the imaginary frequency, calculated to be 578i cm^{-1} , corresponds to the concerted transfer of the hydride to the proximal oxygen of H_2O_2 , lengthening of the peroxide O–O bond, and simultaneous shift of the hydrogen atom from the proximal to the distal oxygen. The result of this rearrangement,

as confirmed by the IRC analysis, is the formation of a hydroxy-amine complex and elimination of one water molecule. Products are more stable with respect to reactants by 68.1 kcal/mol in gas phase (66.3 kcal/mol in acetonitrile). The next step is the intramolecular elimination of a water molecule from the hydroxy-amine that exactly coincides with the second step of pathways (b) and (c) described before, which was demonstrated to be the preferred one.

The reaction occurs via the TS9 transition state for the amine hydrogen transfer to the hydroxide oxygen atom, which lies 52.2 kcal/mol and 47.7 kcal in gas phase and in solvent, respectively, below the energy of the reactants. The regenerated catalyst **1** and water molecules products are calculated to be more stable by 66.3 kcal/mol in gas phase (55.5 kcal/mol in acetonitrile) than the reactants.

We are now in a position to compare the energetics of the O_2 reduction process calculated with and without the involvement of H_2O_2 as intermediate reaction product. The calculated barrier that is necessary to overcome to eliminate the first water molecule directly from the hydroperoxo intermediate by reduction with $\mathbf{1}\text{H}(\text{H})$ is lower than both the barrier to release H_2O_2 from $\mathbf{1}\text{H}(\text{OOH})$ and the barrier to elimination of the first water molecule by reduction of the H_2O_2 product with $\mathbf{1}\text{H}(\text{H})$. Computations, therefore, reveal that the O_2 reductive sequence that does not involve hydrogen peroxide production is energetically preferred.

3.6. O_2 Reduction in Acidic Conditions. We ran calculations also for O_2 reduction by $\mathbf{1}\text{H}(\text{H})$ in acidic conditions, as suggested by one of the referees of the present work. We have identified

Scheme 3. Proposed Catalytic Cycle for the Dioxygen Reduction with CpIrH(TsDPEN) in the Presence of Acid

several possibilities for the examined process, which should constitute a separate work. Here are summarized the outcomes of preliminary calculations carried out so far, whereas calculated PES are reported in the Supporting Information (see Figures S10–S12). A theoretical proposed catalytic cycle for the hydrogenation of molecular oxygen by $Cp^*IrH(TsDPEN)$ in acidic conditions is sketched in Scheme 3.

The first step of the cycle described above, that is, the acid-catalyzed hydrogenation of the 16-electron amido complex **1**, leads to the formation of the 18-electron amino-hydride, which is able to reduce O_2 in the presence of the acid. The reaction proceeds, along both triplet and singlet pathways, with formation of a stable adduct in which oxygen is still far from the complex and the neighboring acid. The next step is the abstraction of the proton from the acid and formation of a hydroxyl moiety that along the singlet path, in analogy with the mechanism in neutral conditions, appears to be coordinated to the metal center through the oxygen bonded to the hydrogen atom. Along the singlet pathway computational analysis clearly shows that a H_2O_2 molecule is released and the $[1H^+]$ cationic complex is restored. Once H_2O_2 is formed, it can further react with **1H(H)** with the involvement of the acid present in the reaction environment.

The outcomes of our computations show that the elimination of water occurs in one step because of the simultaneous transfer to the oxygen atoms of the peroxide of the proton from the acid and the hydride from the metal. The energetics of the calculated pathways, although not definitive, appear to be drastically more favorable than the analogous pathways in neutral conditions. However, all the attempts to intercept, along the triplet pathway, minima and transition states in the region of the PES where the necessary crossing between triplet and singlet reaction profiles occurs were unsuccessful. Alternative, very stable intermediates were intercepted instead (see Figure S12), which could come into play and modify the envisaged mechanism. Nevertheless, we stress that these are initial results and a careful investigation is under way.

Conclusions

On the basis of the experimental observations and the proposed mechanism, the overall catalytic cycle for the hydro-

genation of molecular oxygen to give water using H_2 catalyzed by the iridium transfer hydrogenation catalyst $Cp^*Ir(TsDPEN-H)$ was theoretically investigated with the aid of density functional theory calculations. The first part of the process, that is, the hydrogenation of the catalyst to form the corresponding amino-hydride complex, appears to be hampered by high-energy barriers, which significantly lower when the reaction is acid-catalyzed. The facile deprotonation of the cationic amine-dihydrogen complex, occurring by a proton transfer from the metal center to the counteranion, yields the amino-hydride **1H(H)**.

Dehydrogenation of **1H(H)** by molecular oxygen occurs via the formation of a hydroperoxo intermediate by direct insertion of triplet oxygen 3O_2 into the iridium–hydride bond. Since along the oxygenation pathway the triplet ground-state multiplicity of reactants evolves into the singlet ground-state multiplicity of the hydroperoxo product, a spin crossing has to occur. The reduction of the hydroperoxo complex by unreacted **1H(H)** completes the cycle with the elimination of water and restoring the $Cp^*Ir(TsDPEN-H)$ catalyst, which is poised to be reduced by H_2 . The outcome of our computational analysis shows that the most favorable path for the elimination of water involves, as the first step of the process, formation of hydroxy-amine and water molecules together with the restored catalyst **1** through a concerted mechanism. From the hydroxy-amine complex a second water molecule is eliminated by an intramolecular hydrogen transfer from the amine nitrogen to the oxygen atom. The results reported here suggest that the rate-determining step of the whole hydrogenation process of molecular oxygen catalyzed by a Ir hydrogen transfer complex is the OOH moiety rearrangement to produce the **1H(OOH)** complex along the singlet surface. The calculated energy barrier relative to the transition state for this rate-determining step (17.3 kcal/mol) is in good agreement with the value estimated (18.9 kcal/mol) on the basis of a reaction rate study of the **1H(H) + O₂** process.

The release of H_2O_2 from the **1H(OOH)** intermediate complex appears to be viable. However, computations reveal that the O_2 reductive sequence that does not involve hydrogen peroxide production is energetically preferred.

Finally, some preliminary results concerning the O_2 reduction in acidic conditions show that the O_2 reduction proceeds by

intermediate production of H_2O_2 , which reacts with $1\text{H}(\text{H})$ to eliminate water, restore $[1\text{H}]^+$, and restart the catalytic cycle. The energetics of the process appear to be definitely more favorable with respect the analogous pathways in neutral conditions.

Acknowledgment. This research was supported by Università della Calabria and was carried out within the FP7 project HY-POMAP (project no. 233482).

Supporting Information Available: Selected geometrical parameters for all calculated structures of reactants, intermediates, transition states, and products; preliminary PESs for O_2 reduction in acidic conditions; complete list of authors for refs 18 and 23. Cartesian coordinates and energies of all optimized stationary points. This material is available free of charge via the Internet at <http://pubs.acs.org>.

JA908453K